DRAG PARTITION FOR REGULARLY-ARRAYED ROUGH SURFACES

D. M. CRAWLEY and W. G. NICKLING*
Wind Erosion Laboratory, Department of Geography, University of Guelph, Guelph, Ontario, N1G 2W1, Canada

(Received in final form 28 June 2002)

Abstract. Vegetation and other roughness elements distributed across a surface can provide significant protection against wind erosion by extracting momentum from the flow and thereby reducing the shear stress acting at the surface. A theoretical model has previously been presented to specify the partition of drag forces for rough surfaces and to predict required vegetation density to suppress wind erosion. However, the model parameters have not yet been constrained and the predictive capacity of the model has remained uncertain. A wind-tunnel study was conducted to measure the drag partition for a range of roughness densities and to parameterise the model in order to improve its range of potential applicability. The drag forces acting on both an array of roughness elements and the intervening surface were measured independently and simultaneously using new drag balance instrumentation. A detailed measure of the spatial heterogeneity of surface shear stresses was also made using Irwin sensors. The data agreed well with previous results and confirmed the general form of the model. Analysis of the drag partition confirmed the parameter definition $\beta = C_R/C_S$ (where C_R and C_S are roughness element and surface drag coefficients, respectively) and a constant proportional difference between the mean and maximum surface shear stress was found. The results of this experiment suggest that the definition for m, the surface shear stress inhomogeneity parameter, should be revised, although the theoretical and physical reasons for including this parameter in the model appear to be valid. Best-fit values for m ranged from 0.53 to 0.58.

Keywords: Drag partition, Roughness arrays, Shear stress, Shear stress partitioning, Wind erosion.

List of Symbols

b	roughness element breadth (m)
C_R	roughness element drag coefficient
C_S	surface drag coefficient
F	total force (N)
F_R	force acting on roughness elements (N)
F_S	force acting on surface (N)
H	height (m)
m	surface shear stress inhomogeneity parameter
n	number of roughness elements

* Corresponding author. E-mail: nickling@uoguelph.ca

Boundary-Layer Meteorology **107:** 445–468, 2003.

R	friction velocity/shear stress ratio
R_t	threshold friction velocity/threshold shear stress ratio
R'	mean shear stress ratio
R''	maximum shear stress ratio
S	surface area (m^2)
U_f	freestream wind velocity (m s^{-1})
U_h	wind velocity at height h (m s^{-1})
u_{*tR}	threshold friction velocity for surface protected by roughness elements (m s^{-1})
u_{*tS}	threshold friction velocity for bare, erodible surface (m s^{-1})
β	ratio of roughness element to surface drag coefficients
λ	roughness density
ρ	air density (kg m^{-3})
σ	ratio of roughness element basal to frontal area
τ	shear stress (N m^{-2})
τ_R	roughness element shear stress (N m^{-2})
τ_S	surface shear stress (N m^{-2})
τ_S'	mean surface shear stress acting on intervening area (N m^{-2})
τ_S''	maximum surface shear stress acting on intervening area (N m^{-2})

1. Introduction

Vegetation distributed across a surface can provide significant protection against wind erosion by extracting momentum from the flow and reducing the shear stress acting at the surface (Siddoway et al., 1965; Marshall, 1971; Wolfe and Nickling, 1993). Even when distributed in sparse arrays, vegetation has the potential to reduce or eliminate soil loss by wind. The type, quantity and spatial distribution of vegetation required to attenuate wind erosion has been investigated both empirically and theoretically. In particular, Raupach et al. (1993) proposed a theoretical model that may be used as the basis for predicting required amounts of vegetation to reduce the wind erosion potential. However, the predictive capacity of this model remains uncertain and the protective role of vegetation is yet to be fully understood.

2. Background

The presence of roughness elements, such as vegetation, at the surface increases the total drag and provides a degree of shelter that results in reduced surface shear

stress. The effect of roughness elements on the drag forces and shear stresses at the surface was first studied in detail by Schlichting (1936) who stated that the total drag force F imparted to a rough surface due to fluid flow can be partitioned into a force F_R acting on the roughness elements and a force F_S acting on the surface:

$$F = F_R + F_S. \tag{1}$$

When solved for shear stress the drag partition can be restated as:

$$\tau = \tau_R + \tau_S, \tag{2}$$

where τ_R is roughness shear stress and τ_S is shear stress acting on the underlying surface of area S.

As the quantity of roughness elements is increased for a given surface area, both total drag and roughness drag increase while the force acting on the surface decreases. The drag partition problem is to establish the change in total drag as well as the changes in drag acting on the roughness elements and on the intervening surface as a function of roughness type, size and spacing. Most often, this is described by the roughness density λ, defined as:

$$\lambda = \frac{nbh}{S}, \tag{3}$$

where n is number of roughness elements of width b and height h per unit surface area. In a comprehensive wind-tunnel study, Marshall (1971) measured τ and τ_R for a canopy of roughness elements and placed the concept of drag partition within the wind erosion context. Marshall (1971) found that the stress partition primarily depends on λ and was only slightly dependent on shape and arrangement of the roughness elements.

Raupach (1992) followed this with a theoretical analysis of the drag partition problem that was further defined by Raupach et al. (1993) for the context of soil loss by wind. Raupach et al. (1993) presented a theoretically based model for predicting the protective role of non-erodible roughness elements in terms of a threshold friction velocity ratio R_t (Lyles et al., 1974; Gillette and Stockton, 1989) as a function of roughness geometry at the surface:

$$R_t = \frac{u_{*tS}}{u_{*tR}} = \left[\frac{\tau'_S}{\tau}\right]^{-1} = \left[\frac{1}{(1-\sigma\lambda)(1+\beta\lambda)}\right]^{1/2}, \tag{4}$$

where u_{*tS} is threshold friction velocity for a bare surface, u_{*tR} is threshold friction velocity for the same surface protected by non-erodible roughness elements, τ'_S is shear stress acting on the exposed intervening surface, σ is the ratio of roughness element basal area to frontal area, and $\beta = C_R/C_S$ is the ratio of drag coefficients for an isolated roughness element to bare surface. The parameter β accounts for

roughness element shape effects and entirely controls the drag partition (Raupach, 1992).

Raupach et al. (1993) recognized that other researchers had identified spatially non-uniform erosion patterns around various shapes of roughness elements (e.g., Iversen et al., 1991) and reasoned that the onset of particle movement would not be initiated by the spatially averaged surface shear stress τ_S' but by the maximum shear stress τ_S'' acting on the surface. An empirical assumption was made that τ_S'' for a given surface is equal to τ_S' for a less densely covered surface with the same roughness elements such that:

$$\tau_S''(\lambda) = \tau_S'(m\lambda), \tag{5}$$

where m is an empirical constant ≤ 1 that accounts for the spatial non-uniformity of the surface shear stress distribution. To account for the difference between τ_S' and τ_S'', the parameter m was introduced to Equation (4) and the complete threshold friction velocity ratio was then defined as:

$$R_t = \left[\frac{\tau_S''}{\tau}\right]^{1/2} = \left[\frac{1}{(1 - m\sigma\lambda)(1 + m\beta\lambda)}\right]^{1/2}, \tag{6}$$

where β and m are independent parameters. It is noted in Equation (6) that the drag partition is in large part controlled by the term $(1 + m\beta\lambda)$. In contrast the $(1 - m\sigma\lambda)$ term that provides a correction for the amount of surface covered by the bases of the roughness elements differs little from unity resulting in relatively small changes in R_t. As well, a weakness of the model lies in the fact that m and β are closely related, which may result in collinearity problems. Using appropriate parameters Raupach et al. (1993) found Equation (6) to agree reasonably well with the wind-tunnel data of Gillette and Stockton (1989) (small, erodible spheres and larger, non-erodible hemispheres) and the field data of Musick and Gillette (1990) (porous shrubs, semi-arid environment). Based on the evaluation of the data sets, it was suggested that $\beta \approx 100$ and that $m = 0.5$ for flat erodible surfaces and $m = 1$ for topographically stabilised surfaces.

Wolfe and Nickling (1996) investigated the stress partition problem in a desert shrub community and found $\beta \approx 200$ when they assumed $m = 0.5$. Musick et al. (1996) measured R_t using modelled porous plants in a wind tunnel with an erodible bed of sand and found strongest agreement between their data and Equation (6) when $\beta = 90$ to 180 and $m = 0.5$ to 1 as a function of h/b. For a desert shrub community, Wyatt and Nickling (1997) measured values of τ_S'/τ consistent with the previous findings of Gillette and Stockton (1989) and Musick and Gillette (1990). Independent measurements of C_S and C_R yielded $\beta = 202$ resulting in residual values of 0.14 to 0.18 for m when Equation (6) was resolved. In addition to these primary evaluations of the model, other recent studies have included work by McKenna Neuman and Nickling (1995), Nickling and McKenna

Neuman (1995), Lancaster and Baas (1998), McKenna Neuman (1998) and Nielsen and Aiken (1998).

Although the form of this model is highly practical and is generally supported, related studies have highlighted some uncertainties. Most problematic is that the partition prediction can be made to fit almost any set of data points by adjusting β and m. Empirical derivation of β should be possible, but remains difficult in the field, especially for porous roughness where a clear and practical definition of C_R remains uncertain (Gillies et al., 2000). In addition, Musick et al. (1996) have shown that β has some degree of dependency on aspect ratio that might not otherwise manifest itself in direct measurements of C_R and C_S. Generally, values of β found in empirical studies tend to be larger than that suggested by Raupach et al. (1993). No theoretical or empirical basis has been made for the range of m suggested by Raupach et al. (1993), nor has any detailed investigation of the spatial distribution of surface shear stress been made. Values for m obtained in field and laboratory studies vary widely and inconsistently, possibly due to misrepresentation of other parameters, leaving the meaning and importance of this parameter uncertain from a practical perspective. Without clearly defined parameters, significant overestimation or underestimation of R_t may occur. This seriously impedes the application of the drag partition model in a predictive capacity for remedial wind erosion control.

The purpose of this study was to directly measure the drag partition for a range of roughness canopies in order to parameterise the model of Raupach et al. (1993) and improve its range of predictive applicability. A wind-tunnel investigation was conducted using newly-developed drag balance instrumentation to simultaneously and independently measure the forces acting on the roughness canopy and on the intervening surface. This paper presents the principal findings of the study and a discussion of these within the context of the model and the results of other studies.

3. Methodology

A series of laboratory wind-tunnel experiments was conducted using a model roughness array. New drag balance instrumentation was used in tandem with point measurements of surface shear stresses within the roughness array in order to investigate the stress partition problem for a range of roughness densities and wind speeds. All testing was conducted in the Department of Geography recirculating wind tunnel at the University of Guelph. The working section is approximately 8.0 m long, 0.76 m high, and 0.92 m wide with a surface consisting of smooth, varnished plywood. A pitot tube mounted at 0.37 m above the wind-tunnel surface was used to monitor freestream velocity U_f.

New drag balance instrumentation was developed to measure independently and simultaneously drag forces acting on both an array of roughness elements and the exposed intervening surface within the array. Direct measures of τ_S are rare due to

the difficulty of developing and deploying the necessary instrumentation. Where an estimate of surface shear stress is required, it is typically derived from either eddy correlation methods or from the logarithmic velocity relation in the constant flux layer (Prandtl, 1932). For cases of flow over roughness canopies, these approaches fail to accurately describe the momentum flux and, hence, τ_S within the array (Kaimal and Finnigan, 1994). An accurate estimate of τ_S is essential when the drag force is partitioned between the roughness array and the surface. Typically, investigations of drag partition have derived τ using measured wind velocity above the array. Either one of τ_R or τ_S has then been quantified using a variety of direct and indirect measures, leaving the remaining term to be resolved residually. Direct measures of both τ_R and τ_S have not previously been made in studies of the drag partition.

Various designs of drag meters have been used in both laboratory and field investigations of forces on roughness elements and flow over rough surfaces (e.g., Bradley, 1968; Marshall, 1971; Thom, 1971; Gillies, 1994; Stacey et al., 1994; Wyatt and Nickling, 1997; Grant and Nickling, 1998; Gillies et al., 2000; Nemoto and Nishimura, 2001). The instrument developed here consists of two independent translational surfaces attached to a stationary base with bearing-mounted lever arms (Figures 1 and 2). An outer open rectangular frame provides the first translational surface and surrounds the second, inner surface (Figure 2). In this configuration, force could be applied to either surface, and then measured, independently of the other surface. In order to measure applied forces, loading points were taken directly off each of the translational surfaces and directly connected to load cells from Metler model BD1201 electronic balances sensitive to $\pm 10^{-4}$ kg (Figure 2). The drag balance instrument was levelled and aligned approximately 0.125 m below the wind tunnel (Figure 1b) and in the end portion of the working section (Figure 1a). A surface plate was then attached to the outer balance and a roughness array mounted to the inner balance. Equal mass counterweights were used to dampen the dynamic response of the balances and prevent potential oscillatory motion.

The surface plate was 1.78 m $\times$ 0.6 m and was constructed of 6.4-mm thick plywood, reinforced from below to prevent wind-induced vibrations. It was directly connected to the translational surface of the outer drag balance, allowing direct transfer of the applied force to the strain gauge. The inner drag balance allowed measurement of drag forces on the roughness arrays. Removable mounting posts of 6.4 mm diameter and 0.075 m height were positioned on the roughness drag balance along each of two offset grid patterns and extended vertically up through small clearance holes in the surface plate by approximately 0.012 m. An annular gap of approximately 0.002 to 0.003 m surrounded the surface plate and the clearance holes. This aperture was large enough to ensure clearance for fitting but still small enough to ensure negligible jetting effects (Bradley, 1968). Each drag balance was calibrated in place for applied force by connecting the surface plate

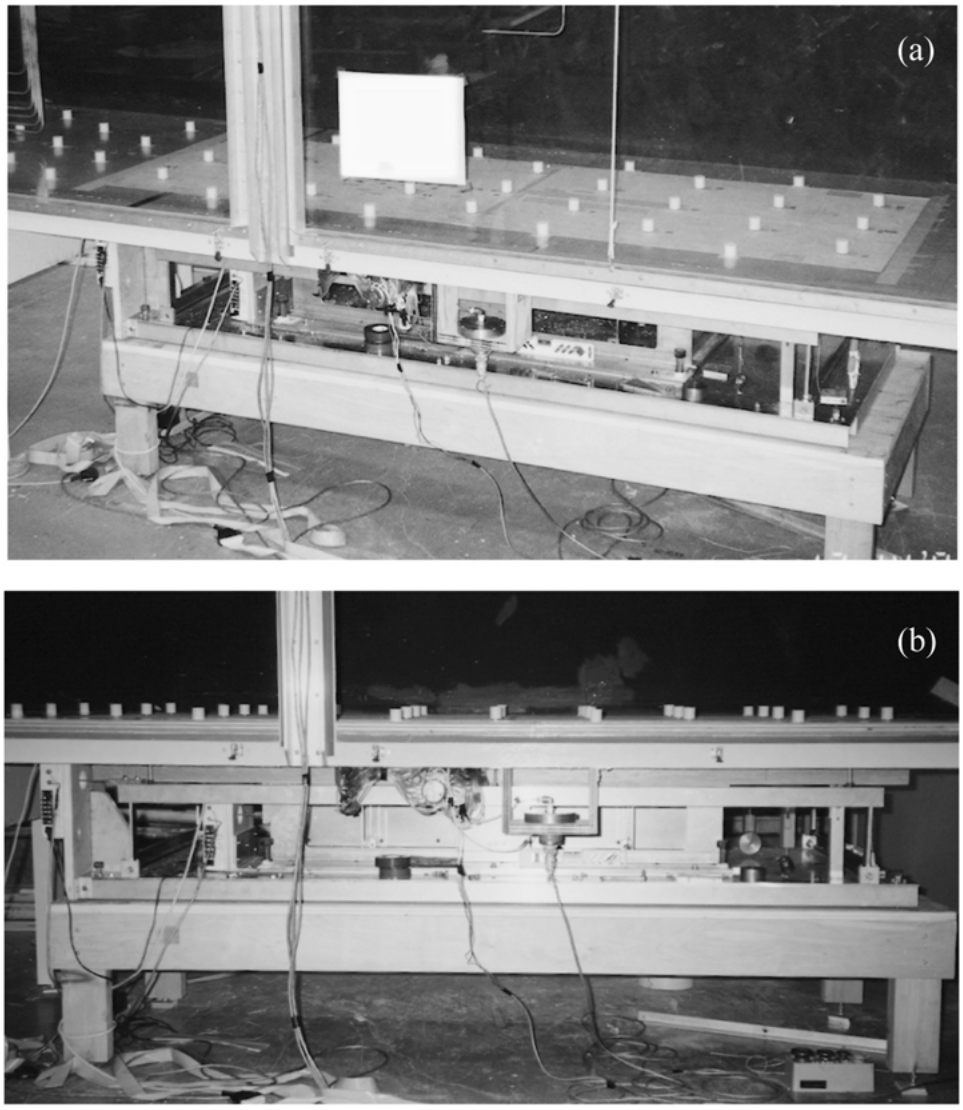

Figure 1. (a) Wind-tunnel testing configuration with drag balance instrumentation in place. (b) Detail of drag balance instrumentation.

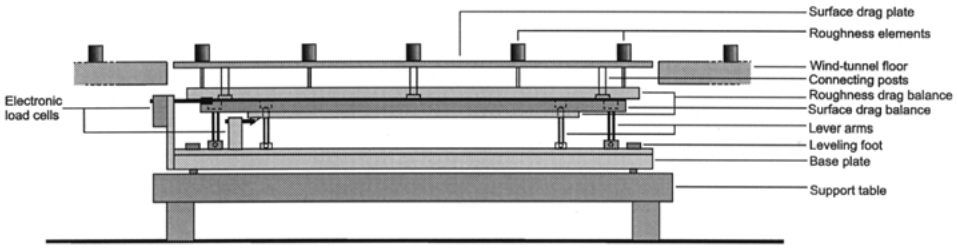

Figure 2. Schematic diagram of the drag balances.

to vertically suspended precision weights. A strong linear response ($r^2 = 0.9993$ to 0.9999) was found for the performance of the balances.

The roughness array used in the wind-tunnel tests consisted of vertically-oriented polystyrene foam cylinders, chosen for their ease of use, relatively constant C_R (Taylor, 1988), clearly defined frontal area, and previous usage in comparable studies (e.g., Kutzbach, 1961; Marshall, 1971; Lyles et al., 1974; Lyles and Allison, 1976; Raupach et al., 1980; Iversen et al., 1991; Musick et al., 1996). The roughness elements extended 11 rows upwind of the drag balances. Roughness elements mounted to the drag balance were positioned with a slight clearance ($<$ 0.001 m) between their bottom surface and the surface drag plate.

Although it would have been preferable to have more than 11 rows of roughness elements mounted upwind of the drag balances to ensure equilibrium flow conditions, the number of rows was constrained by the length of the wind-tunnel working section. For the element configuration used, the fetch-length to element-height ratio is on the order of 100, providing an internal boundary-layer depth of approximately 5–10 roughness element heights, which is relatively shallow for this type of study. The relatively shallow boundary-layer depth and lack of equilibrium flow conditions over the roughness surface could result in larger shear stresses reaching the bed than would be expected for equilibrium flow conditions. In an earlier study simulated vegetation elements of similar size and spacings as the polystyrene cylinders were used to investigate the effect of fetch length on surface shear stress and drag force on the elements within the simulated vegetation (Nickling et al., 1999). Although wind speed dependent, it was found that for the range of free stream wind speeds used, surface shear stress within the simulated vegetation did not change significantly after the addition of 8–10 rows of roughness elements upwind of the surface shear stress measurements. Although more rows of roughness elements upwind of the drag balances would have been desirable we are confident that the configuration used does provide adequate flow conditioning to be representative of equilibrium flow conditions.

To directly measure the spatial distribution of surface shear stress and to quantify τ_S'', an array of Irwin sensors was configured within the roughness array. The Irwin sensor is a simple, omni-directional skin friction meter that measures the near-surface vertical pressure gradient (refer to Irwin, 1980, for complete specifications). Once calibrated, the Irwin sensor can be used to measure surface shear stress at frequencies greater than 10 Hz (Irwin, 1980; Wu and Stathopolous, 1994) and has been successfully deployed in a variety of flow conditions and settings (Irwin, 1980; Wu and Stathopolous, 1994; Monteiro and Viegas, 1996; Wyatt and Nickling, 1997). The differential in dynamic pressure is measured between two ports, one at the surface and one at a height of 0.00175 m above the surface.

An array of Irwin sensors was mounted on the surface drag plate at 23 nodal locations along a regular, evenly-space 4 $\times$ 6 grid within the roughness array (where the 24th node is the position of the roughness element). The grid covers the rectangular region between two diagonally offset roughness elements, and is rep-

TABLE I
Summary of wind-tunnel roughness array geometry.

λ	h (m)	b (m)	σ	h/b
0.0064	0.024	0.024	0.79	1.0
0.00642	0.017	0.034	1.57	0.5
0.0096	0.036	0.024	0.52	1.5
0.0118	0.023	0.046	1.57	0.5
0.0128	0.034	0.034	0.79	1.0
0.0144	0.024	0.024	0.79	1.0
0.0145	0.017	0.034	0.79	0.5
0.0193	0.051	0.034	1.57	1.5
0.0216	0.036	0.024	0.52	1.5
0.0235	0.046	0.046	0.79	1.0
0.0289	0.034	0.034	0.79	1.0
0.0434	0.051	0.034	0.52	1.5

resentative of the full surface stress field, with the assumption that the stress field is self-repeating within the array. This assumption is valid for regularly distributed roughness arrays with uniform geometry. Each Irwin sensor was connected with 0.5 m of flexible tubing to a Scanivalve that sequentially connected each sensor to a Viatran model 219-12 differential pressure transducer. The sensors were calibrated for surface shear stress *in situ* against the surface drag balance when no roughness array was present. The differential pressure measured by the Irwin sensors was found to be most strongly related by a power function to surface shear stress as measured by the drag balance ($r^2 \geq 0.9824$).

Twelve roughness array configurations were tested comprised of: two centre-to-centre spacings (0.2 m and 0.3 m), 3 diameters (0.024 m, 0.034 m, 0.046 m) and 3 aspect ratios (0.5, 1, 1.5) providing a range of λ from 0.0064 to 0.0434. Table I provides details of the λ configurations tested. Each array was tested over a range of six pre-selected freestream velocities: 7.11, 9.57, 11.63, 14.53, 17.07, and 19.29 m s^{-1}. Two replications at each array configuration were made for a total of 144 runs; each run lasted 496 sec, with a 2-sec sampling interval.

4. Results

Measured drag forces were normalised by the exposed surface area of the surface drag plate and the frontal area of the roughness array, respectively, as surface shear stress τ_S' and roughness shear stress τ_R. The drag balance measured τ_S' and τ_R

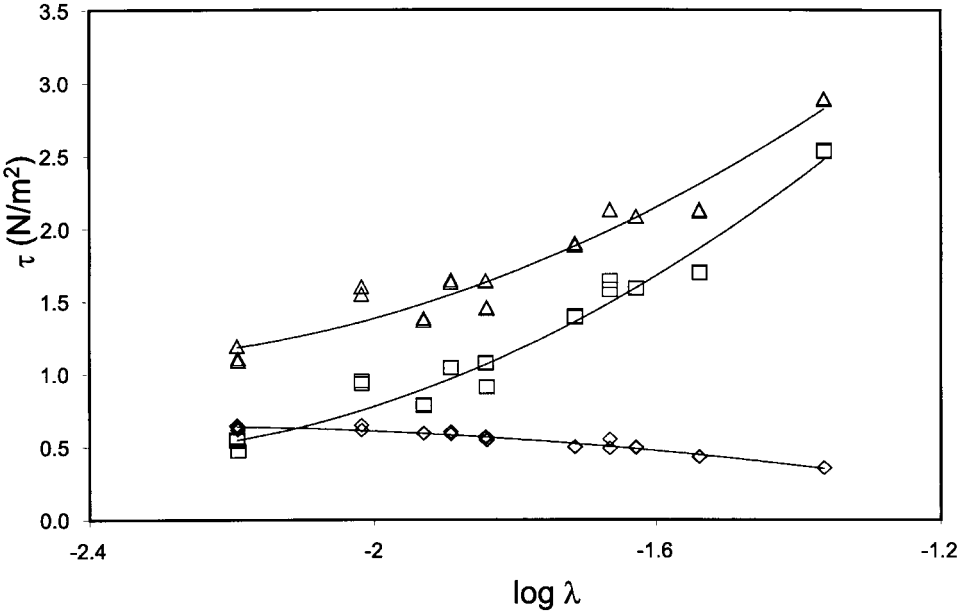

Figure 3. Drag balance measured shear stress partition as a function of λ for U_f = 19.29 m s^{-1}.

allowed calculation of total shear stress τ using Schlichting's (1936) statement of drag partition. As expected, τ_R increased while τ_S decreased with increasing λ. Figure 3 shows a representative example of the change in τ, τ_S and τ_R as a function of λ for U_f = 19.29 m s^{-1}. Both τ and τ_R increased in magnitude and converged somewhat with increasing λ, while τ_S decreased. The relative rate of change in these trends highlights the two principal results of adding roughness to a surface as noted by Musick et al. (1996): the primary effect of increasing λ is to increase the total shear stress while only secondarily it reduces the shear stress acting at the surface.

The drag balance measured shear stress partition terms then allowed calculation of R for non-threshold conditions defined by Wolfe and Nickling (1996) as:

$$R = \left(\frac{\tau_S'}{\tau}\right)^{1/2}, \tag{7}$$

where τ here is the total shear stress measured by the drag balances. Following the convention used in previous literature calculated values of R are plotted against log λ in Figure 4 along with Marshall's (1971) data set. The calculated R decreases approximately log-linearly from 0.8 to 0.3 as λ increases from 0.0064 to 0.0434. The degree of scatter in the data for each λ is very low, indicating that the drag partition is independent of U_f. In addition, the scatter for the entire data set is low, which further confirms Marshall's (1971) finding that the drag partition is well described by λ for these kinds of roughness elements (e.g., cylinders, cubes;

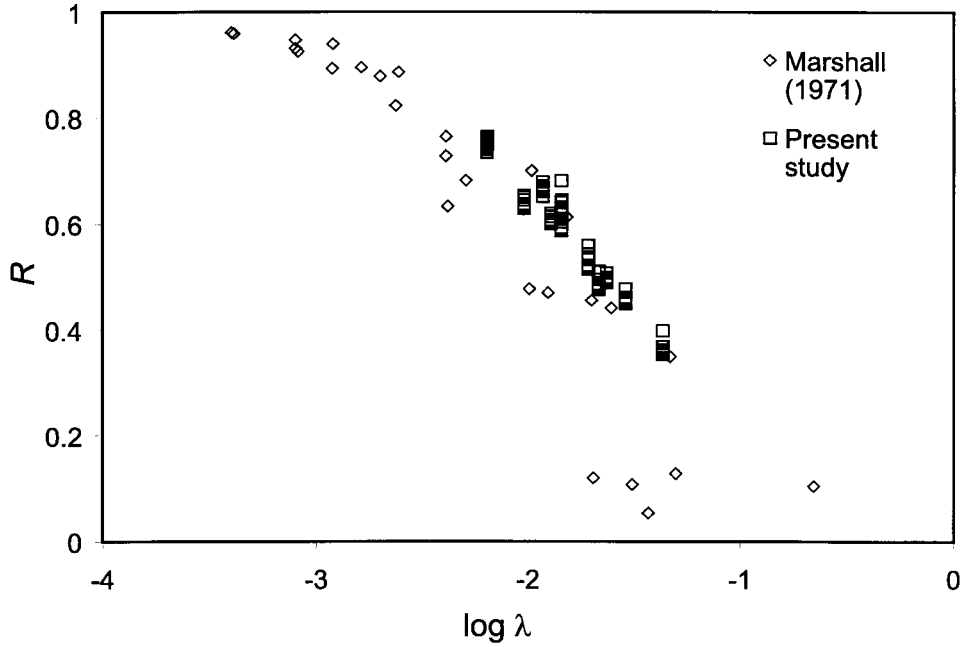

Figure 4. Comparison of measured mean surface shear stress ratios.

greater degrees of scatter potentially may occur for other roughness shapes and structures). The drag-balance-measured stress partition is generally in good agreement with the results of Marshall (1971). A greater degree of scatter is evident in Marshall's (1971) results over the range of λ where the data sets overlap, with some values of R falling lower than observed here. However, with the exception of the outliers where $R < 0.1$, which may result from measurement limitations, the data essentially describe the same relationship.

Although the general drag partition for turbulent flow over a roughness array can be specified reasonably by the temporally and spatially-averaged mean drag forces, the spatial heterogeneity of surface shear stresses was characterised in order to fully evaluate the model of Raupach et al. (1993). In order to ensure that the Irwin sensor grid samples were an accurate indicator of surface shear stress within the array, τ_S' measured by the Irwin sensors was used to calculate the shear stress ratio R':

$$R' = \left(\frac{\tau_S'}{\tau}\right)^{1/2}, \tag{8}$$

where τ here is the total shear stress measured by the drag balances. In this case, τ_S' measured by the Irwin sensors was calculated as the arithmetic mean of the 23 point measurements located within the array. A comparison of measured shear stress ratios is shown in Figure 5. Excellent agreement was found between the Irwin sensor and drag balance measured shear stress ratios ($r^2 = 0.9602$).

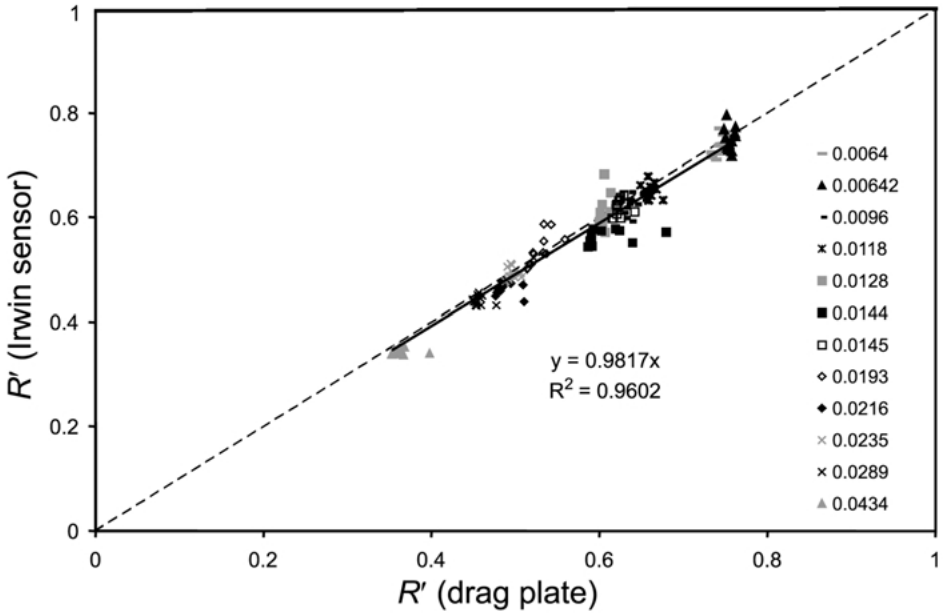

Figure 5. Comparison of R' measured by drag balance and Irwin sensor instruments.

In order to represent the stress partition predicted by Equation (6) and to understand the change in the shear stress ratio R due to the difference between τ_S'' and τ_S' as a function of λ, τ_S'' was resolved from the distribution of shear stress. Both τ_S'' and τ_S' are plotted as a function of λ for a representative case in Figure 6. For all cases, τ_S'' and τ_S'' decrease logarithmically as λ increases, although the magnitude of this change decreases slightly as U_f increases. In addition, the slope of the relationship between τ_S'' and λ was found to be slightly greater than that for τ_S', suggesting that as λ decreases, the difference between τ_S'' and τ_S' decreases. This is largely as expected since, when $\lambda = 0$, τ_S'' should equal τ_S'.

The relationship between τ_S'' and τ_S' was further examined with the direct comparison of paired values of τ_S'' and τ_S' for all tests shown in Figure 7. A very strong linear relationship ($r^2 = 0.9801$) was found to describe the difference between τ_S'' and τ_S' over the range of λ tested. A constant proportional difference exists with $\tau_S'' = 1.3455\tau_S'$ independent of both λ and U_f. The maximum measured surface shear stress τ_S'' within the array for each test was then used to calculate the surface shear stress ratio R'':

$$R'' = \left(\frac{\tau_S''}{\tau}\right)^{1/2}, \tag{9}$$

where τ here is total shear stress measured by the drag balance, as in Equation (8). A comparison of the observed R'' values and other experimental results where the stress partition is specified in terms of τ_S'' is presented in Figure 8. Measured values

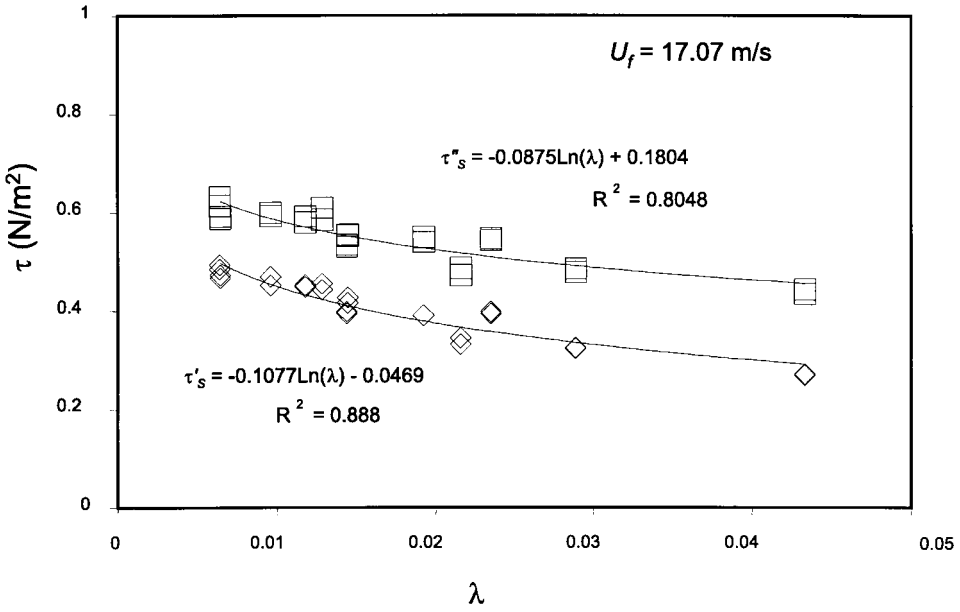

Figure 6. Observed mean (τ'_S) and maximum (τ''_S) surface shear stress plotted as a function of λ and U_f with logarithmic regression functions shown for a representative wind speed.

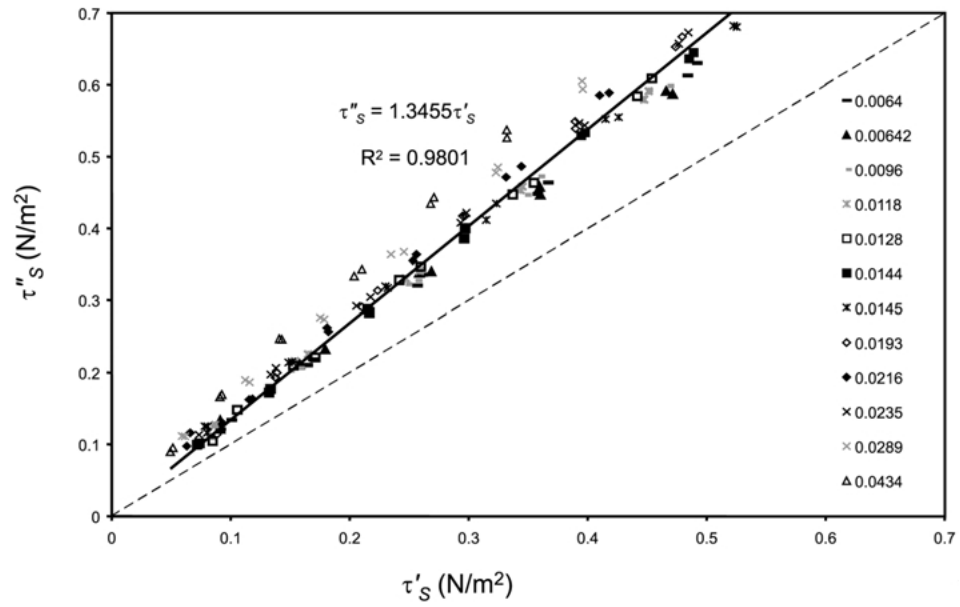

Figure 7. Comparison of Irwin sensor measured mean τ'_S and maximum τ''_S surface shear stress (N m^{-2}).

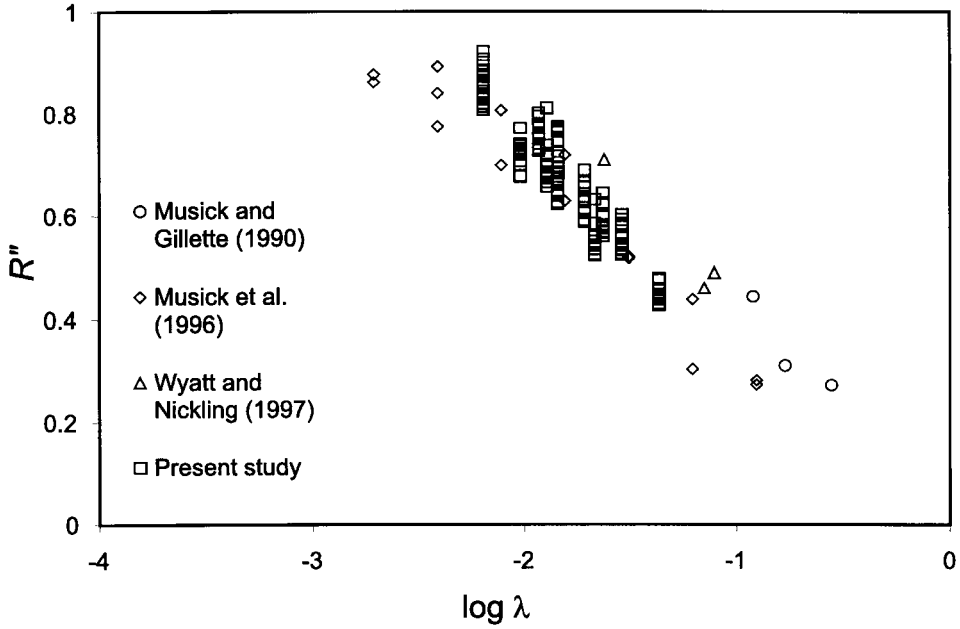

Figure 8. Comparison of measured maximum surface shear stress ratios.

for R'' decrease from about 0.85 to 0.4 as λ increases from 0.0064 to 0.0434. The results of the wind-tunnel experiment are consistent with the results of Musick and Gillette (1990), Musick et al. (1996), and Wyatt and Nickling (1997). Although there is some scatter in the data, likely as a function of small aspect ratio changes, the stress partition is remarkably consistent over a range of scales and roughness element types (e.g., solid cylinders, modelled porous elements, shrub vegetation). These observations define the same trend as shown in Figure 4, but $R'' > R$ for the sameλ. The agreement between the observed R'' and these other results, especially for those where the stress partition was explicitly measured at particle threshold, validates both the Irwin sensor measure of the surface stress distribution as well as the assumption of Raupach et al. (1993) that the erosion threshold occurs as a function of τ_S'' within the array. As such, the specification of the stress partition in terms of τ_S'' is confirmed and the theoretical reasons for introducing a parameter to the general stress partition prediction to account for the surface stress heterogeneity can be considered valid.

5. Analysis and Discussion

With the drag balance and Irwin sensor measurements, it was possible to evaluate the conceptual and theoretical basis and definitions of both β and m. For both cases, independent estimates of the parameter value were made using the above

definitions. As well, the measured R, R' and R'' data allowed residual solutions for both β and m to provide the best-fit of Equation (6) to the observations, forming the basis for direct evaluation of each parameter, and an overall evaluation of the shear stress model.

5.1. THE β PARAMETER

5.1.1. *Independent Definition Solutions to β*

Raupach (1992) stated that the stress partition is controlled entirely by β. As such, it remains the most important factor to be determined in order to constrain accurately the prediction. A solution to β independent of Equations (4) and (6) and other parameters was found using $\beta = C_R/C_S$ as suggested by Raupach et al. (1993). Here, C_R is determined for an isolated, unobstructed roughness element while C_S is found for the bare surface in the absence of roughness elements from:

$$C_S = \frac{\tau_S}{\rho U_h^2}. \tag{10}$$

Over the range of U_f, C_S values ranged from about 0.0020 to 0.0025. Exact values for β for each test were then determined using $C_R = 0.3$ as suggested by Taylor (1988) for a cylinder, and calculated C_S values specific to each tested roughness geometry and wind speed. With this approach, β values fall between approximately 110 to 160 with no apparent dependence on λ, and mean $\beta = 140$, slightly less than $\beta = 170$ found for Marshall's (1971) study due to the higher C_S here. When the independent mean $\beta = 140$ is used to resolve Equation (4), strong agreement ($r^2 = 0.9458$) is found with the drag-balance-measured shear stress ratio R. In this case, R is defined for τ_S' by Equation (4) and, as such, m is not included in the prediction. Solutions for β using the drag balance measurements were also resolved specific to each roughness element aspect ratio as suggested by Musick et al. (1996). When considered separately, β was found to be 149, 141, 127 for σ = 0.52, 0.79, 1.57, respectively. The predictions fit the observed R reasonably well, although the agreement decreases slightly as σ increases (r^2 = 0.9773, 0.9521, 0.8303, respectively).

5.1.2. *Residual Solutions to β*

Alternately, β was solved residually from Equation (4) for exact values using both the drag balance measured R and Irwin sensor measured R'. Comparison of these residual values for β to the independent values from above allowed evaluation of the β definition for the model. An iterative non-linear regression routine was used to resolve Equation (4) for various β in order to find the least sum of squares best-fit to the measured R data. This approach yielded an overall best-fit β = 131, with β = 147, 130, 113 for σ = 0.52, 0.79, 1.57, respectively, and provided a high degree of agreement with the observed stress partition (r^2 = 0.9587 overall, and r^2 = 0.9778, 0.9752, 0.9802, for each σ respectively).

This residual approach was also used to find the β values that provide the best-fit prediction of Equation (4) to the Irwin sensor R' data. In this case, $\beta = 139$ for all data, while $\beta = 158, 140, 117$ for $\sigma = 0.52, 0.79, 1.57$ respectively ($r^2 = 0.9295$ overall, with $r^2 = 0.9265, 0.9597, 0.8866$, for each σ respectively). The slightly lower agreement reflects the greater degree of scatter in the Irwin sensor measured R' compared to the drag balance R observations.

5.1.3. *Evaluation of β Solutions*

When the overall independent solution of $\beta = 140$ is compared to the drag-balance residual least squares solution of $\beta = 131$, the independent parameterisation of β was found to overestimate the best-fit case by 6.9%. The independent estimate of $\beta = 140$ was found to be closer to the Irwin sensor residual $\beta = 139$, an overestimate of only 0.7%. In addition, when aspect ratio specific solutions are considered, the agreement between the independent and residual solutions ranged from an underestimate of 7.0% to an overestimate of 12.4%.

When both the overall and aspect ratio specific cases are considered, the agreement between the independent estimate of β and the residual solution required to satisfy the model is generally very good, with the greatest difference of approximately 12%. However, since no direct measure of C_R was made in this study, this difference is at least partially dependent on the independent estimate of $C_R = 0.3$ (Taylor, 1988). The inherent degree of uncertainty in this estimate of C_R was $\pm 25\%$ (Taylor, 1988). Given that the residual C_R values and the overall discrepancy in β values were well within this range of uncertainty, the parameterisation of $\beta = C_R/C_S$ in the drag partition model can thus be considered accurate when used with Equation (4) to predict the general stress partition.

In the initial evaluation of the model, Raupach et al. (1993) used $\beta = C_R/C_S$ to predict R_t and found good agreement with the data of both Marshall (1971) and Gillette and Stockton (1989). However, a single value of σ was used regardless of h/b for the Marshall (1971) data. Raupach (1992) did note some dependency on h/b in Marshall's drag partition data set, and suggested that this dependency could be accounted for by adjusting values of β, most probably by varying C_R with aspect ratio. This dependency on h/b was further investigated in detail by Musick et al. (1996) who found that by varying β as a function of h/b better agreement between the prediction and the observations was possible. However, no measured C_S was presented by Musick et al. (1996) and the choice of β was largely arbitrary. Although aspect ratio was not varied over a great range in these previous studies, the results of the present investigation further indicate that there is some slight degree of β dependency on roughness element aspect ratio. In the present case, this only resulted in a $\pm 12\%$ variation in β despite a $\pm 50\%$ change in aspect ratio. The dependence on aspect ratio can be attributed to the combined effects of slight resultant changes in C_S as a function of the specific reference height for wind speed U_h as well as some change in C_R as a direct function of changing aspect ratio. However, the nature of this relationship cannot be explicitly determined here.

Although the pattern of agreement between the independent and residual solutions to β for the aspect ratio specific cases varies depending on the instrumentation used to measure the stress partition, the magnitude of the variation is well within the overall estimate of uncertainty. As such, for roughness canopies where aspect ratio does not vary greatly, no correction to $\beta = C_R/C_S$ should be required.

5.2. THE *m* PARAMETER

5.2.1. *Independent Definition Solution to* m

Using the parameter definition (Equation (5)), a solution to m was found independently of the form of the stress partition specification and of other parameters (e.g., β) with the Irwin sensor data set. The observed relationships between τ_S'', τ_S' and λ shown in Figure 6 provide support for the theoretical expectation of the stress distribution. As expected, a noticeable convergence was found between τ_S'' and τ_S' as $\lambda \to 0$. However, this convergence is small, especially considering the scatter in the data and the relative effect of the data points at $\lambda = 0.0434$. Logarithmic regression relations were used in the analysis of m because of both good fit and convergence of the τ_S'' and τ_S'' curves as $\lambda \to 0$, although there is no theoretical basis for this form of the relation, nor data to support the trend at either low or high λ. Following the parameter definition, these paired logarithmic regression relationships were set equal to each other. An iterative procedure was then used to solve the paired relations for m using Equation (5) over the range of known surface stresses and λ. As shown in Figure 9a, solution values for m decrease rapidly as a power function with increasing λ and seem to approach an asymptote value of 0.2 to 0.3 for $\lambda > 0.01$. This results in a relatively constant value for m within the range of λ observed within this study, although some dependence on U_f was apparent, with higher values for m found as U_f increases for $\lambda > 0.01$. In addition, the regression relationships predict that the curves for m converge as $\lambda \to 0$. However, there is some error here, as values for m were found to exceed 1 for very small λ. This is likely an artefact of the error associated with extending the solution to the logarithmic regression relations beyond the range of tested λ, which leads to the prediction of unrealistically high shear stress for the convergence of τ_S' and τ_S'' as $\lambda \to 0$. Mean values for m for all U_f were taken as a function of λ, making it possible to predict R'' using Equation (6). The predicted R'' from the independent β and m is shown with observed data in Figure 9b. When the independent solution to m is used with Equation (6), the predicted R'' greatly overestimates the observations for all but the lowest observed λ and becomes progressively worse for increasing λ.

5.2.2. *Residual Solutions to* m

An alternate parameterisation for m was also made using an iterative approach to find exact residual solutions for m from the Irwin sensor derived R' and R'' and Equation (6). This approach has the primary advantage of providing a solution that

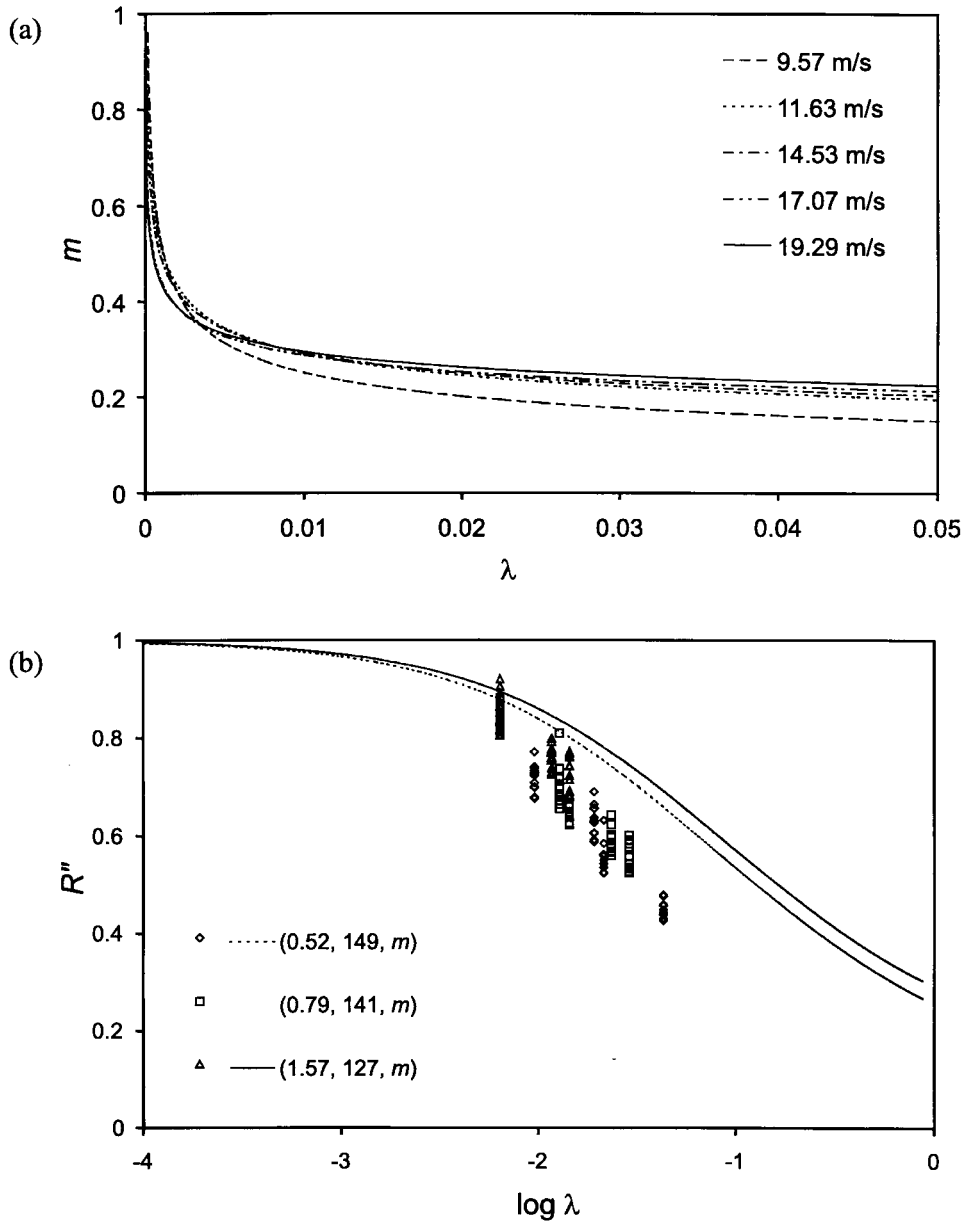

Figure 9. (a) Parameter definition solution to m. Solutions are plotted as a function of λ and are grouped by U_f. (b) Predicted R'' using independent solutions for β and m shown with observed R'' data for comparison. Here the solution m is a wind-speed averaged function of λ.

satisfies both the general stress partition (Equation (4)) and the physical requirement of specifying the partition in terms of τ_S'' at erosion threshold (Equation (6)) without any *a priori* assumptions in defining m (e.g., as in Equation (5)).

Two solutions were made. The first relied on the independent derivation of β from the parameter definition using $C_R = 0.3$ and a case-specific C_S for each test. Using the best-fit residual values for β and the measured R'' values, Equation (6) was solved for m using an iterative non-linear regression analysis. This resulted in $m = 0.57$ for all data, while $m = 0.62, 0.58, 0.48$ for $\sigma = 0.52, 0.79, 1.57$, respectively. A high degree of agreement between the observed and predicted R'' was found, with $r^2 = 0.8769$ overall, and $r^2 = 0.8972, 0.8980, 0.7205$ for respective aspect ratios.

The second approach to solving for m used the residual β values. To find m, the calculated R'' values were resolved using Equation (6) and the exact best-fit β values. Exact m solutions are shown as a function of λ in Figure 10a. Here, m ranges from 0.35 to 0.65 with some scatter both for individual λ cases and across all λ, although no clear pattern exists as a function of λ. In this case, $m = 0.58$ when $\beta = 139$ for the entire data set, and $m = 0.58, 0.58, 0.53$ for $\sigma = 0.52, 0.79, 1.57$, respectively. The R'' prediction is shown in Figure 10b along with the observed R'' values. A high degree of agreement between the observed and predicted R'' is evident, with an overall $r^2 = 0.8769$ and aspect ratio specific $r^2 = 0.8972, 0.8980, 0.7205$, respectively.

5.2.3. *Evaluation of* m *Solutions*

Although both the independent and residual analyses show some dependency on U_f, the independent parameterisation quite drastically underestimates the values of m required to fit Equation (6) to the observed R'' over the range of λ. The parameter definition of m provided in Equation (5) must therefore be rejected as incorrect and inadequate to account for the surface stress heterogeneity. Although there is some scatter in the residual solution, m is reasonably constant over the range of observed λ. This is consistent with the result that a constant proportional relationship exists between τ_S' and τ_S'' (e.g., Figure 7). With an overall value of $m = 0.58$, the residual solution is relatively consistent with the suggested value of $m = 0.5$ for a flat, erodible surface (Raupach et al., 1993).

Although τ_S'' can be described as a function of τ_S' for a less dense roughness array, there is no theoretical or physical basis to expect the shear stress ratio to be described adequately in these terms. Most significantly, by using this approach, where the stress partition at a particular λ is described for a lower λ, the change to the total shear stress, which increases as a function of roughness density, is not adequately accounted for. This results in an underestimation of m when the parameter is defined as in Equation (5). Given that the effect of m becomes greater with smaller values in defining R_t, the accurate representation of this parameter is essential to the predictive capacity of the model. Underestimation of m leads

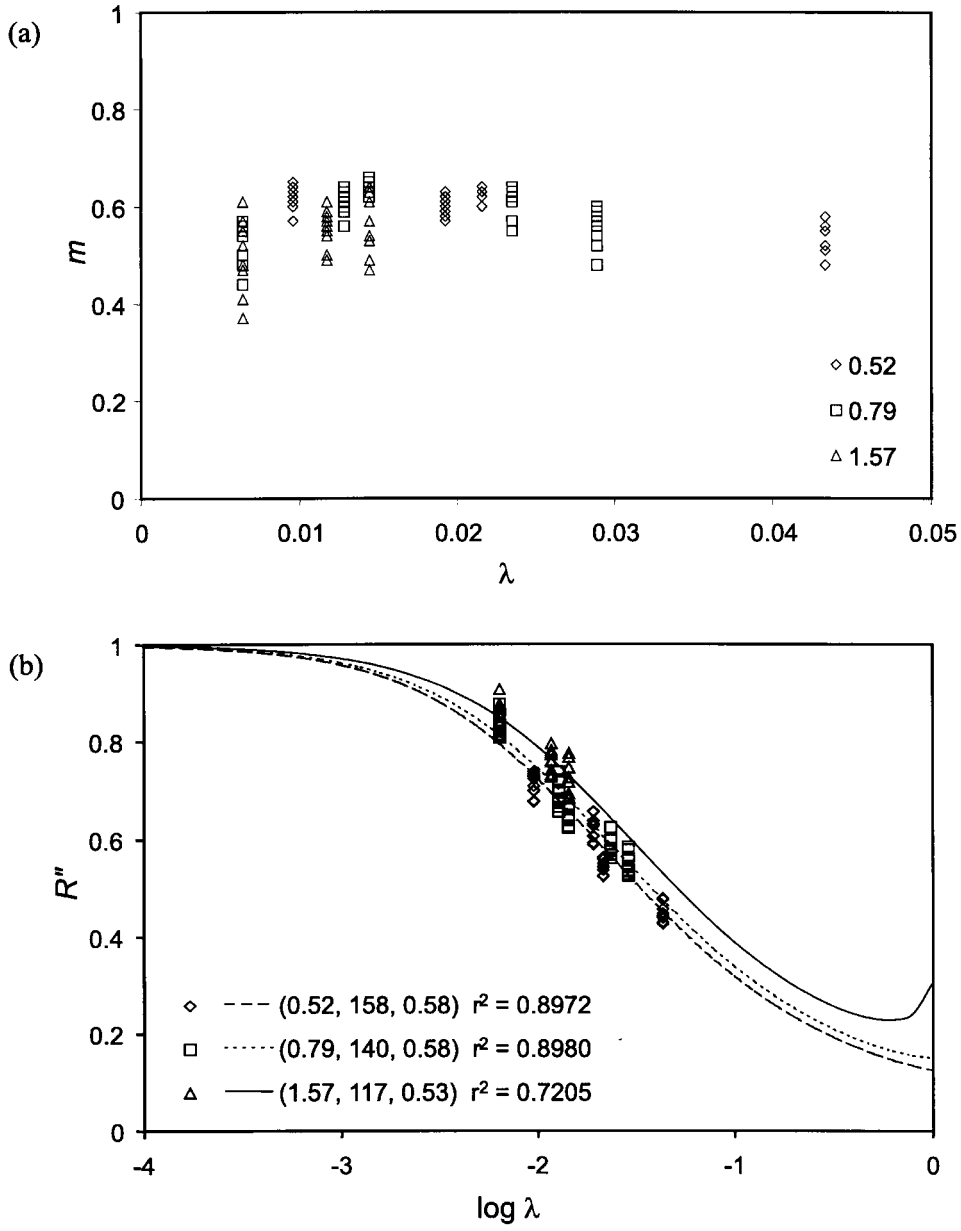

Figure 10. (a) Exact solutions to m derived from Irwin sensor measured R'' and exact residual β. (b) Observed R'' Irwin sensor measured stress partition shown with the predicted R'' using the best-fit regression β and m. Results are grouped by (σ, β, m).

to increasing overestimation of λ to satisfy a given threshold condition, which in practice may result in unnecessary practical difficulties and economic costs.

The physical meaning of the m parameter and how it might be independently defined remains to be addressed. Other studies have typically assigned $m = 0.5$ or $m = 1$. For any given λ, increasingly smaller values for m must reflect greater increases in τ_S'' compared to τ_S', and hence R'' compared to R'. The low value of $m = 0.16$ reported by Wyatt and Nickling (1997) suggests that in their sparse vegetation array τ_S'' exceeded τ_S' by a greater factor than found in the present study. This may be a real effect of flow dynamics influenced by porous roughness elements where extended wake development may result in negatively skewed surface stress distributions with comparatively reduced τ_S''. Alternately, this may be attributable to measurement error, either in misdefining τ_S'' due to the limited number of Irwin sensors deployed in the field or in the estimate of β due to practical problems with determining C_R for porous obstacles.

For studies where bed erosion was used to determine the stress partition, m has been suggested to range from 0.5 to 1 as a function of topographically influenced surface stability. Raupach et al. (1993) found $m = 1$ for the data sets of Lyles and Allison (1976) and Iversen et al. (1991). However, for these studies, a fluid threshold was found as emerging lag conditions led to a stabilized surface, resulting in an increased u_{*tR} compared to that observed for a flat bed (Raupach et al., 1993). For these cases, m was used to account for an apparent increase in τ_S' rather than a real change in the difference between τ_S' and τ_S''. Therefore, use of $m = 1$ is not recommended.

The remaining data (Gillette and Stockton, 1989; Musick and Gillette, 1990; Musick et al., 1996) suggest that $m = 0.5$. This is in good agreement with the resolved values for m presented here. As such, $m = 0.5$ to 0.6 can be confidently used to predict the shear stress partition. In addition, these values are empirically based indicators of the spatial heterogeneity of surface shear stresses. As such, the parameter still satisfies the theoretical and physical reasoning for which it was introduced to the model. However, with the rejection of the parameter definition (Equation (5)), there is now no independent basis from which to define m. Variation in m outside of this range of values remains a realistic potential effect of changes in the nature of roughness elements, and, hence, within-array airflow. The spatial distribution of surface shear stresses can be expected to be influenced by the type of flow separation and wake diffusion developed for different roughness types. In particular, the specific effects of roughness element porosity and flexibility are still largely unquantified (Gillies et al., 2000). However, there is some support for this range of values for m in cases of porous roughness elements (Musick and Gillette, 1990; Musick et al., 1996).

Although the model and its parameters have been clearly defined within the original framework, some caution must still be exercised in applying the model. There is still relatively little field data from which to inform an evaluation of the unique drag characteristics of vegetation roughness elements, such as porosity and

flexibility, and any consequent changes to β or m, especially for particle threshold conditions. Leaf fluttering, re-orientation and streamlining can lead to geometric changes and the distribution of plant surface area may be variable both vertically and horizontally, including situations where basal area $\rightarrow 0$ for a single stem plant (e.g., creosote). It is not yet clear how these factors will change C_R, and hence β and the drag partition for actual vegetation arrays (Gillies et al., 2000). Similarly, these factors may cause changes to the surface stress distribution leading to potential variability in m. As such, some uncertainty in the predictive capacity of the model for cases of soil erosion by wind remains to be addressed.

6. Conclusions

The results of this study provide a parameterisation to the theoretical specification of drag partition presented by Raupach et al. (1993) and improve its range of predictive applicability.

There are several principal findings of this study. First, the measured shear stress partition indicated that the general specification of the drag partition derived by Raupach (1992) is valid. In addition, the parameterisation $\beta = C_R/C_S$ was found to be correct when compared to a residual solution.

A high degree of agreement was found between the measured R'' stress partition and other observed R_t results. This suggests that both the practical and theoretical reasons for defining the stress partition in terms of the maximum surface shear stress are correct and that the introduction of an additional parameter to the general stress partition prediction is valid. A constant proportional relationship between the mean and maximum surface shear stress was found independent of wind speed over the range of roughness densities examined, such that $\tau_S'' = 1.3455\tau_S'$.

From an analysis of the spatial heterogeneity of surface shear stress within the roughness array, the definition for m suggested by Raupach et al. (1993) appears incorrect. However, the theoretical and physical reason for including this parameter (i.e., to account for the difference between τ_S' and τ_S'' at the onset of particle entrainment) remains valid. When the parameter definition was solved it was found to underestimate the residual best-fit values for m, which ranged from approximately 0.5 to 0.6. This range of values is generally consistent with previously reported values. Therefore, the use of $m = 0.6$ is recommended to account for the spatial heterogeneity of surface shear stresses when predicting R''. Variation outside the range $m = 0.5$ to 0.6 remains a realistic possibility for vegetation canopies.

Lastly, the parameters β and m appear to be somewhat aspect-ratio dependent, although this effect was considerably less than previously suggested by Musick et al. (1996). It is questionable whether this effect is significant enough to warrant direct consideration in specifying the stress partition, especially for cases when the aspect ratio does not vary greatly from unity.

Acknowledgements

We would like to express our appreciation to Jack Gillies and Nick Lancaster for many fruitful discussions on wind erosion and shear stresses in sparse vegetation communities. We are also grateful to Mario Finoro for outstanding technical support and guidance, and to Ian Walker for assistance with the Irwin sensors. Special thanks are also extended to two anonymous reviewers for their very insightful comments that added greatly to this paper. Funding from the Natural Sciences and Engineering Research Council of Canada in the form of an operating grant to WGN and a graduate scholarship to DMC is gratefully acknowledged.

References

Bradley, E. F.: 1968, 'A Shearing Stress Meter for Micrometeorological Studies', *Quart. J. Roy. Meteorol. Soc.* **94**, 380–387.

Gillette, D. A. and Stockton, P. H.: 1989, 'The Effect of Nonerodible Particles on Wind Erosion of Erodible Surfaces', *J. Geophys. Res.* **94**, 12885–12893.

Gillies, J. A.: 1994, *A Wind Tunnel Study of the Relationship Between Complex Surface Roughness Form, Flow Geometry and Shearing Stress*, Ph.D. Dissertation, University of Guelph, Canada, 231 pp.

Gillies, J. A., Lancaster, N., Nickling, W. G., and Crawley, D. M.: 2000, 'Field Determination of Drag Forces and Shear Stress Partitioning Effects for a Desert Shrub (*Sarcobatus vermiculatus*, Greasewood)', *J. Geophys. Res.* **105**, 24871–24880.

Grant, P. F. and Nickling, W. G.: 1998, 'Direct Field Measurement of Wind Drag on Vegetation for Application to Windbreak Design and Modelling', *Land Degrad. Dev.* **9**, 57–66.

Irwin, H. P. A. H.: 1980, 'A simple Omnidirectional Sensor for Wind-Tunnel Studies of Pedestrian Level Winds', *J. Wind Eng. Ind. Aerodyn.* **7**, 219–239.

Iversen, J. D., Wang, W. P., Rasmussen, K. R., Mikkelson, H. E., and Leach, R. N.: 1991, 'Roughness Element Effect on Local and Universal Saltation Transport', *Acta Mech. Suppl.* **2**, 65–75.

Kaimal, J. C. and Finnigan, J. J.: 1994, *Atmospheric Boundary Layer Flows: Their Structure and Measurement*, Oxford University Press, New York, 283 pp.

Kutzbach, J. E.: 1961, 'Investigation of the Modification of Wind Profiles by Artificially Controlled Surface Roughness', in *Studies of Three-Dimensional Structure of the Planetary Boundary Layer*, *Annual Report Contract DA-36-039-SC-80282.* Department of Meteorology, University of Wisconsin, Madison, WI, pp. 71–113.

Lancaster, N. and Baas, A.: 1998, 'Influence of Vegetation Cover on Sand Transport by Wind: Field Studies at Owens Lake, California', *Earth Surf. Proc. Landforms* **23**, 69–82.

Lyles, L. and Allison, B. E.: 1976, 'Wind Erosion: The Protective Role of Simulated Standing Stubble', *Trans. AMSE* **19**, 61–64.

Lyles, L., Schrandt, R. L., and Schmeidler, N. F.: 1974, 'How Aerodynamics Roughness Elements Control Sand Movement', *Trans. AMSE* **17**, 134–139.

Marshall, J. K.: 1971, 'Drag Measurements in Roughness Arrays of Varying Density and Distribution', *Agric. Meteorol.* **8**, 269–292.

McKenna Neuman, C.: 1998, 'Particle Transport and Adjustments of the Boundary Layer over Rough Surfaces with an Unrestricted, Upwind Supply of Sediment', *Geomorphology* **25**, 1–17.

McKenna Neuman, C. and Nickling, W. G.: 1994, 'Momentum Extraction with Saltation: Implications for Experimental Evaluation of Wind Profile Parameters', *Boundary-Layer Meteorol.* **68**, 35–50.

Monteiro, J. P. and Viegas, D. X.: 1996, 'On the Use of Irwin and Preston Wall Shear Stress Probes in Turbulent Incompressible Flows with Pressure Gradients', *J. Wind Eng. Ind. Aerodyn.* **64**, 15-29.

Musick, H. B. and Gillette, D. A.: 1990, 'Field Evaluation of Relationships between a Vegetated Structural Parameter and Sheltering against Wind Erosion', *Land Degrad. Rehabil.* **2**, 87–94.

Musick, H. B., Trujillo, S. M., and Truman, C. R.: 1996, 'Wind-Tunnel Modelling of the Influence of Vegetation Structure on Saltation Threshold', *Earth Surf. Proc. Landforms* **21**, 589–605.

Nemoto, M. and Nishimura, K.: 2001, 'Direct Measurement of Shear Stress during Snow Saltation', *Boundary-Layer Meteorol.* **100**, 149–170.

Nickling, W. G. and McKenna Neuman, C.: 1995, 'Development of Desert Lag Surfaces', *Sedimentology* **42**, 403–414.

Nickling, W. G., Gillies, J. A., Lancaster, N., and Crawley, D. M.: 1999, *Optimizing Managed Vegetation Planting Configurations at Owens Lake*, *California*, Final Technical Report to Great Basin Unified Air pollution Control District, Bishop, CA, 76 pp.

Nielson, D. C. and Aiken, R. M.: 1998, 'Wind Speed above and within Sunflower Stalks Varying in Height and Population', *J. Soil Water Cons.* **53**, 347–352.

Prandtl, L.: 1932, 'Zur turbulenten Strömung in Röhren und längs Platten', *Ergebn. Aerdyn. Versuchsanst.* **4**, 18–29.

Raupach, M. R.: 1992, 'Drag and Drag Partition on Rough Surfaces', *Boundary-Layer Meteorol.* **60**, 375–395.

Raupach, M. R., Gillette, D. A., and Leys, J. F.: 1993, 'The Effect of Roughness Elements on Wind Erosion Threshold', *J. Geophys. Res.* **98**, 3023–3029.

Raupach, M. R., Thom, A. S., and Edwards, I.: 1980, 'A Wind-Tunnel Study of Turbulent Flow Close to Regularly Arrayed Rough Surfaces', *Boundary-Layer Meteorol.* **18**, 373–397.

Schlichting, H.: 1936,'Experimentelle Untersuchungen zum Rauhigkeitsproblem', *Ingen.-Arch.* **7**, 1–34; *NACA Tech. Mem.* 823.

Siddoway, F. H., Chepil, W. S., and Armbrust, D. V.: 1965, 'Effect of Kind, Amount, and Placement of Residue on Wind Erosion Control', *Trans. AMSE* **8**, 327–331.

Stacey, G. R., Belcher, R. E., and Wood, C. J.: 1994, 'Wind Flows and Forces in a Model Spruce Forest', *Boundary-Layer Meteorol.* **69**, 311–334.

Stockton, P. H. and Gillette, D. A.: 1990, 'Field Measurement of the Sheltering Effect of Vegetation on Erodible Land Surfaces', *Land Degrad. Rehabil.* **2**, 77–85.

Taylor, P. A.: 1988, 'Turbulent Wakes in the Atmospheric Boundary Layer', in W. L. Steffen and O. T. Denmead (eds.), *Flow and Transport in the Natural Environment: Advances and Applications*, Springer-Verlag, Berlin, pp. 270–292.

Thom, A. S.: 1971, 'Momentum Absorption by Vegetation', *Quart. J. Roy. Meteorol. Soc.* **97**, 414–428.

Wolfe, S. A. and Nickling, W. G.: 1993, 'The Protective Role of Sparse Vegetation in Wind Erosion', *Prog. Phys. Geog.* **17**, 50–68.

Wolfe, S. A. and Nickling, W. G.: 1996, 'Shear Stress Partitioning in Sparsely Vegetated Desert Canopies', *Earth Surf. Proc. Landforms* **21**, 607–619.

Wu, H. and Stathopoulos, T.: 1994, 'Further Experiments on Irwin's Surface Wind Sensor', *J. Wind Eng. Ind. Aerodyn.* **53**, 441–452.

Wyatt, V. E. and Nickling, W. G.: 1997, 'Drag and Shear Stress Partitioning in Sparse Desert – Creosote Communities', *Can. J. Earth Sci.* **34**, 1486–1498.